Preprint typeset in JINST style - HYPER VERSION

MICE-NOTE-XXX
October 20, 2014

Measurement of the pion contamination in the Muon Ionisation Cooling Experiment (MICE) beam *

M. Bogomilov
Department of Atomic Physics, St. Kliment Ohridski University of Sofia, Sofia, Bulgaria

M. Bonesini
Sezione INFN Milano Bicocca, Dipartimento di Fisica G. Occhialini, Milano, Italy

D. Orestano, L. Tortora
Sezione INFN Roma Tre e Dipartimento di Matematica e Fisica, Università di Roma Tre, Roma, Italy

O.M. Hansen [1]
CERN, Geneva, Switzerland
[1] *Also at University of Oslo, Norway*

Y. Karadzhov
Department of Atomic Physics, St. Kliment Ohridski University of Sofia, Sofia, Bulgaria
DPNC, Section de Physique, Université de Genève, Geneva, Switzerland

R. Bayes, J.C. Nugent, F.J.P. Soler
School of Physics and Astronomy, Kelvin Building, The University of Glasgow, Glasgow, UK

ABSTRACT: The international Muon Ionisation Experiment (MICE) will perform a systematic investigation of ionisation cooling of a ~ 200 MeV/c muon beam. A low pion contamination in the MICE muon beam is an essential requirement for a precise measurement of ionisation cooling. Data were taken in the MICE "Step I" configuration in order to commission the MICE particle identification detectors and to characterise the MICE beam. The pion contamination in the MICE muon beam is found to be 1% or below, at the entrance of the cooling channel, as expected from Monte Carlo simulations and measured by the MICE particle identification system using a statistical method.

KEYWORDS: Muon Ionisation Cooling; Neutrino Factory; Muon Collider; MICE; Muon Beam.

*version 1: 16/10/2014. **Analysis note for paper to be submitted to JINST**

Contents

1. Introduction

The international Muon Ionisation Cooling Experiment (MICE) [1], under construction at the Rutherford Appleton Laboratory (RAL), will demonstrate the principle of ionisation cooling as a technique for reduction of the phase-space volume occupied by a muon beam. Ionisation cooling channels are required for neutrino factories [2, 3, 4, 5, 6] and muon colliders [7, 8, 9].

Ionisation cooling [10] is accomplished by passing the muon beam through a low-Z material (the "absorber"), in which it loses energy via ionisation, reducing both the longitudinal and transverse components of momentum. The lost energy is restored by accelerating the beam such that the longitudinal component of momentum is increased while the transverse component remain unchanged. The net effect is to reduce the divergence of the beam, hence the volume of transverse phase space that it occupies. Beam transport through the absorbers and accelerating structures is achieved using a solenoid focusing lattice. While a modest cooling factor (~ 3.4) is needed in the current neutrino factory design [6], much greater ($\sim 10^6$) cooling is needed for a muon collider.

2. MICE Apparatus

A schematic diagram of the MICE experiment is shown in figure 1. The MICE cooling channel, which is based on a single lattice cell of the cooling channel described in [11], comprises three 20 litre volumes of liquid hydrogen and two linear accelerator modules (LINAC) each consisting of four 201 MHz cavities, with gradients of $\sim$ 10 MV/m. The superconducting "focus coils" focus the beam into the liquid-hydrogen absorbers, while a "coupling coil" surrounds each of the linac modules.

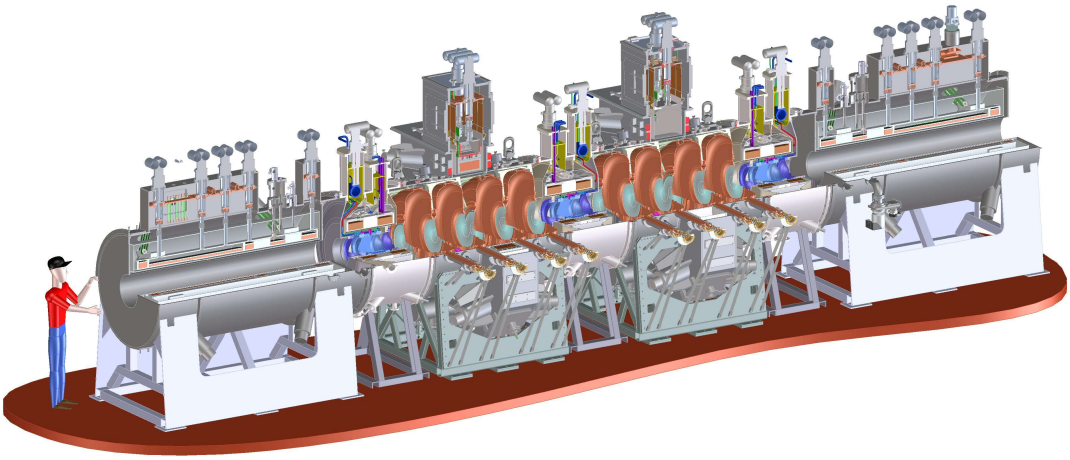

Figure 1. Schematic view of the MICE apparatus: the cooling channel, with its three liquid hydrogen absorbers and two RF cavity modules, is sandwiched between two identical trackers, inside superconducting solenoids. The muon beam is incident from the left. The sequence of solenoids defining the MICE optics is also visible. The cooling cell starts at the first Focus Coil.

A reduction in normalised emittance of 10% is expected for a muon beam entering the cell with a nominal momentum of 200 MeV/c and an emittance $\varepsilon_N = 6.2\pi$ mm$\cdot$rad. To allow extrapolation to a full cooling channel, the instrumentation upstream and downstream of the cooling cell is required to measure this change in emittance, $\Delta\varepsilon_N$, with a relative precision $\Delta\varepsilon_N/\varepsilon_N = 1\%$; i.e., measurements of ε_N upstream and downstream of the cooling cell with an absolute precision of 0.1% are required. Conventional emittance measurement techniques based on beam-profile monitors barely reach a 10% precision.

In order to achieve the required precision, MICE has been designed as a single-particle experiment, in which each muon is measured using state-of-the-art particle detectors and the bunched muon-beam is reconstructed offline [1].

The instrumentation upstream of the MICE cooling cell includes a particle identification (PID) system, that allows a pure muon beam to be selected. The PID system consists of scintillator time-of-flight x/y hodoscopes TOF0 and TOF1 [13] read at both edges by fast conventional Hamamatsu R4998 photomultipliers [14], and two threshold Cherenkov counters Ckova and Ckovb [15]. The

[1] A preliminary application of this method to characterize MICE beams, using only the time-of-flight detectors, has been studied and is reported in reference [12]

TOF system is required to reject pions in the incoming muon beam with an efficiency in excess of 99%. In addition, the precision of the TOF time measurement must be sufficient to allow the phase at which the muon enters the RF cavities to be determined to 5°. To satisfy these requirements, the resolution of each TOF station must be ~ 50 ps. The two Cherenkov detectors have been designed to guarantee muon-identification purities better than 99.7% in the momentum range 210 MeV/c to 365 MeV/c [16]. Both the TOF system and the Cherenkov system, giving only a velocity measurement, may be used for single particle identification once momentum of the incoming particles has been determined precisely. This may be done only in MICE Step IV [17], where the first tracker station [18] will measure momentum of the incoming particles [19]. For MICE Step I a preliminary determination of the pion contamination of the muon MICE beam was obtained on a statistical basis combining the TOF velocity information with the calorimetric KL information.

Downstream of the cooling channel, a final scintillator time-of-flight x/y hodoscope (TOF2 [20]) and a calorimeter system allow muon decays to be identified and rejected. The calorimeter system is composed of a lead-scintillator section (KL), similar to the KLOE design [21] but with thinner lead foils, to be followed soon by a fully active scintillator detector (the electron-muon ranger, EMR) in which the muons are brought to rest. Charged-particle tracking in MICE will be provided by two solenoidal spectrometers in which the position and momentum of each muon is measured before and after the cooling cell.

The KL detector is the most downstream part of the MICE Step I apparatus. It is designed to serve as a preshower for the EMR detector; however, in 2011 the EMR was still under construction. The main role of the KL and EMR detectors is to distinguish muons from decay electrons, but they can separate muons from pions and electrons more generally. KL is a sampling calorimeter, composed of scintillating fibers and extruded Pb foils with active volume of $93 \times 4 \times 93$ cm^3. KL has 21 cells and 42 readout channels. Light from its scintillating fibers is collected by 42 Hamamatsu R1355 PMTs. The PMT signals are sent via a shaper module to 14 bit CAEN V1724 flash ADCs. The shapers stretch the signal in time in order to match the flash ADC sampling rate. A detailed description of KL is given in [19].

The MICE instrumentation must perform efficiently in the presence of background induced by X-rays produced in the RF cavities and must operate in the presence of stray fringe fields from magnets. For a full description of the experiment see [22]. Thus far, only the PID instrumentation and the MICE beam line have been installed (MICE Step I). They are fully described in [19].

3. MICE Muon Beam and 2011 data-taking

In order to avoid detrimental effects on muon emittance measurement, the MICE beam line must deliver muon beams with a pion contamination of less than few per-cent. The required transverse emittance range is $3 \leq \varepsilon_N \leq 10$ π mm $\cdot$ rad, with mean momenta $140 \leq p_\mu \leq 240$ MeV/c and r.m.s. momentum widths of ~ 20 MeV/c; the full range of emittance is required over the full range of momentum. A tungsten or brass "diffuser" of variable thickness is placed at the entrance to the upstream spectrometer solenoid in order to generate the divergence necessary for the required range of emittance.

The design of the MICE muon beam is reported in [19]; we summarize it here briefly (see figure 2). Pions produced by the momentary insertion of a titanium target [23] into the ISIS proton

beam are (1) captured using a quadrupole triplet (Q1–3) and (2) transported to a first dipole magnet (D1), which directs particles of a desired momentum bite into the decay solenoid (DS); (3) muons produced by pions decaying in the DS are momentum-selected using a second dipole magnet (D2) and (4) focused onto the diffuser by a quadrupole channel (Q4–6 and Q7–9). By capturing pions of transverse momentum up to ~ 70 MeV/c, and increasing their path length by deflecting them onto helical trajectories, the decay solenoid increases the probability of muon capture between D1 and D2 by an order of magnitude compared to a simple quadrupole channel. In positive-beam running, a borated polyethylene absorber of variable thickness is inserted into the beam just downstream of DS in order to suppress a high rate of protons [24].

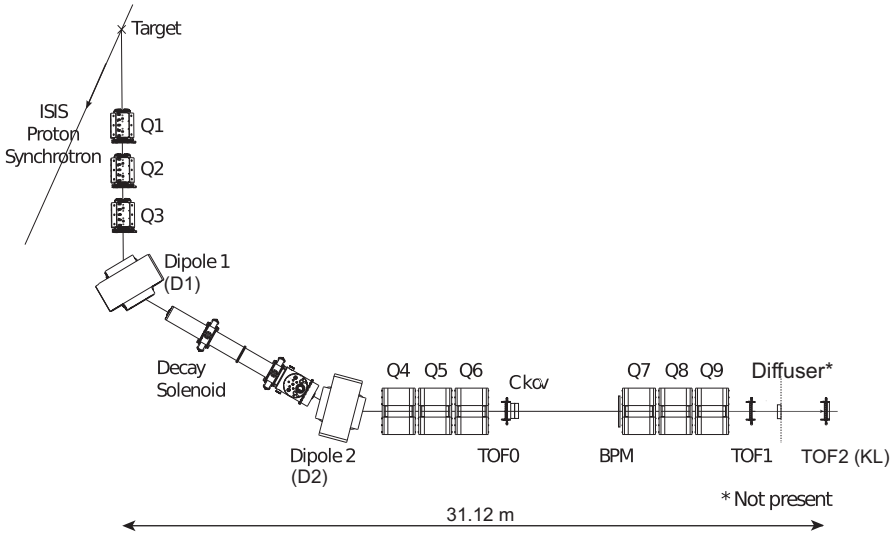

Figure 2. Top view of the MICE beam line with its instrumentation, as used in Step I. The distances between TOF0 (TOF1) and TOF1 (TOF2) are respectively 773.3 cm and 198.8 cm.

The composition and momentum spectra of the beams delivered to MICE are determined by the interplay between the two bending magnets D1 and D2. In normal ("$\pi \to \mu$ mode," or "muon") operation, D2 is set to half the momentum of D1, selecting backward-going muons in the pion rest frame and producing an almost pure muon beam. The simulated momentum distribution at TOF0 for the beam particles in a positive 6π mm 200 Mev/c muon beam is reported in figure 4-c. Undecayed pions at high momentum clearly prevent particle identification on a single-particle basis, in absence of a precise momentum measurement, with either TOF or Cherenkov velocity measurements.

Alternatively, by setting $p_{D1} \simeq p_{D2}$, a mixed beam containing π, μ, and e is obtained. This "calibration mode" is used to calibrate the PID detectors.

The nominal values of the beam momenta p_μ are those evaluated at the centre of the central liquid-hydrogen absorber in the final Step VI configuration. For example, $p_{D2} = 238$ MeV/c gives a p_μ value of 200 MeV/c, the momentum decrease from D2 to the MICE cooling cell being primarily due to energy loss in the material of the PID detectors, the diffuser, and, for positive (+ve) beams,

Table 1. Summary of runs used in this analysis. The muon runs correspond to a nominal setting $(\varepsilon_N, p_\mu) = 6\pi mm \cdot rad$, 200 Mev/$c$. Reported momenta are at the entrance of the quoted detectors.

p_{D2} (MeV/c)	p_{TOF0} (MeV/c)	p_{TOF1} (MeV/c)	p_{TOF2} (MeV/c)	# events (10^3)
calibration runs				
222	217	194	181	195
258	254	231	219	235
280	276	254	242	167
294	290	268	257	354
320	316	295	284	265
362	358	337	326	448
muon runs				
238	220	204	190	270

the proton absorber. The correspondence between beam momenta at various points in the MICE apparatus is summarized in table 1.

MICE Step I data were taken in Dec. 2011 with the apparatus setup shown in figure 2, including the upstream PID detectors and the downstream TOF2 and KL detectors, which were operated in a temporary position about 2 m downstream of TOF1. After refurbishing of TOF0 and TOF1, where the older PMT assemblies were replaced, and after performing a detector calibration, the obtained TOF resolutions were 55 ps for TOF0, 53 ps for TOF1 and 50 ps for TOF2 [25],[26]. Table 1 summarizes the runs used in this analysis.

4. Contamination in the MICE muon beam

4.1 Monte Carlo simulations

The pion contamination under the muon peak was estimated using the G4beamline simulation package [27], developed by Muons, Inc., and by using the MICE Applications User Software (MAUS) package [28] to simulate detector response. The position of all the beam line and detector elements in the beam is given in Table 2.

Figure 3 shows distributions of the time-of-flight between TOF0 and TOF1. Figure 3-a shows data taken with a positive $\pi \to \mu$ beam with a nominal momentum of 200 MeV/c, which has only a small contamination of electrons and pions. Similar beams will be used to demonstrate ionisation cooling. Figure 3-b shows data taken with a calibration beam with $p_{D2} \simeq 222$ MeV/c. In this beam configuration, momentum selected electrons, muons and pions fall into three well-defined peaks. In the $\pi \to \mu$ beam, while e/μ separation is never a problem, the level of the π contamination under the μ peak may be difficult to assess, as the two distributions overlap.

Figure 4 (left) compares distributions of flight time from TOF0 to TOF1, obtained in typical beam configurations, for reconstructed positive-beam data and corresponding to Monte Carlo simulations of a 6π mm $\cdot$ rad positive muon beam with nominal beam momentum $p_\mu = 200$ MeV/c, compared to data. There is a mismatch in the position of the electron peak that needs to be corrected in order to make a full comparison. Figure 4 (right) shows the momentum distribution at TOF1 of the electron, pion and muon peaks for the same Monte Carlo simulation. The correction

Table 2. Position of the MICE beam line elements and detectors for the pion contamination runs during Step I data taking.

Element	Distance from target along beam axis (cm)
Q1	3000.0
Q2	4400.0
Q3	5800.0
D1	7979.1
Decay Solenoid	12210.7
Proton absorber	14880
GVA1	15050.0
D2	15808.1
Q4	17661.6
Q5	18821.6
Q6	19981.6
TOF0	21088.0
Ckova	21251.5
Ckovb	21910.9
Q7	25293.7
Q8	26453.7
Q9	27613.7
TOF1	28793.1
TOF2	31198.1
KL	31323.1

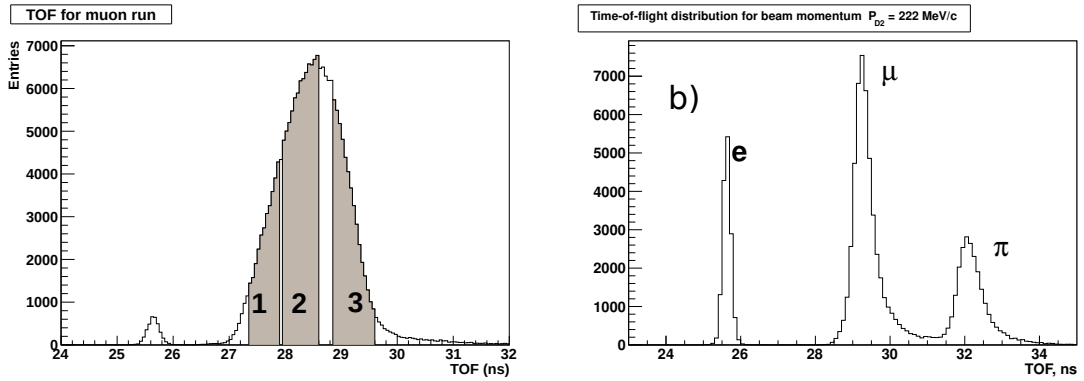

Figure 3. Time of flight between TOF0 and TOF1 for a positive muon beam with a nominal momentum of 200 MeV/c used in the following the analysis (a) and a positive "calibration" beam taken with $p_{D2} = 222$ MeV/c (b). In panel (a) the left peak is due to electrons, the pion contamination will be studied in three time-of-flight intervals, highlighted in grey.

to take into account the difference in the time-of-fight of electrons in data and Monte Carlo is:

$$\frac{\left(\frac{\Delta t_{\mu/\pi}}{\Delta t_e}\right)_{MC}}{\left(\frac{\Delta t_{\mu/\pi}}{\Delta t_e}\right)_{data}} = \frac{\sqrt{1+\left(\frac{m^2_{\mu/\pi}}{p^2_{\mu/\pi}}\right)_{MC}}}{\sqrt{1+\left(\frac{m^2_{\mu/\pi}}{p^2_{\mu/\pi}}\right)_{data}}}, \tag{4.1}$$

where $m_{\mu/\pi}$ is the mass of the muon or pion, $p_{\mu/\pi}$ is the momentum of the muon or pion, $\Delta t_{\mu/\pi}$ is the time-of-flight of the muon or pion and Δt_e is the time-of-flight of the positron. The contamination under the muon peak is summarised in figure 5. The pion contamination at TOF0 is 1.78%, at TOF1 it is 0.38% and at KL it is 0.25%, increasing slowly with momentum.

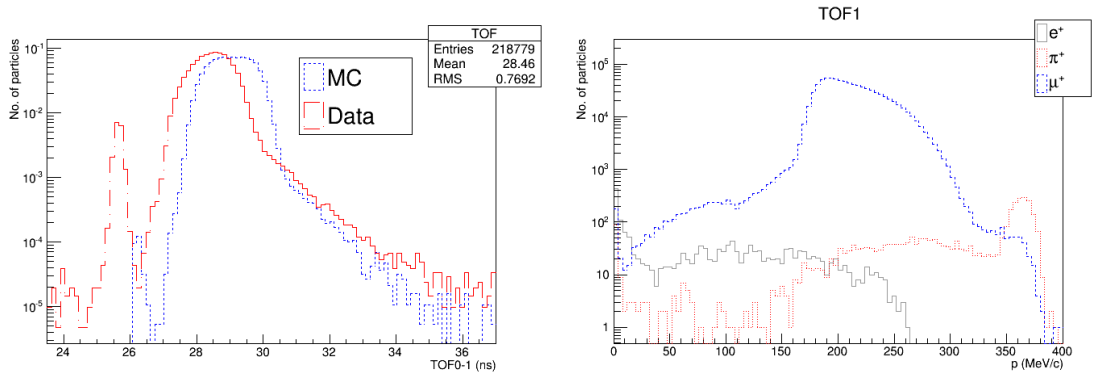

Figure 4. Left: Time-of-flight distributions between TOF0 and TOF1 for data and Monte Carlo simulation for a 6π mm $\cdot$ rad positive muon beam with nominal beam momentum $p_\mu = 200$ MeV/c. Right: Momentum distribution for beam particles at TOF1 for a simulated positive 6π mm $\cdot$ rad at 200 MeV/c (a cut between 26.2 and 32 ns on the time–of–flight between TOF0 and TOF1 is applied).

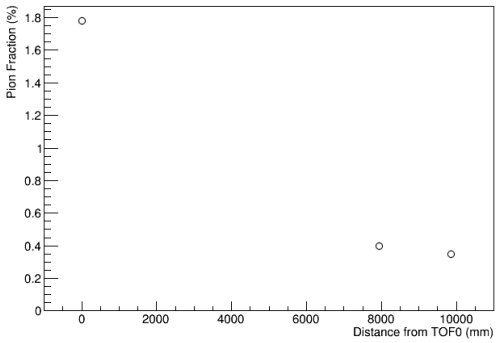

Figure 5. Pion contamination in a 6π mm $\cdot$ rad positive muon beam, at momentum $p_\mu = 200$ MeV/c at different positions along the beam line as deduced from G4beamline and MAUS Monte Carlo simulations. The three points refer to the position of the TOF0, TOF1, and KL positions in the MICE Step I configuration. The z coordinate is in mm in the MICE reference system, where zero is at the target position. The simulation includes a proton absorber of 83 mm. A cut between 26.2 and 32 ns on the time–of–flight between TOF0 and TOF1 is applied.

4.2 Pion contamination measurement with TOF and KL detectors

4.2.1 TOF detector distributions

The residual pion contamination in the beam, after the selection of the muon component via time-of-flight, can be measured from the spectrum of energy released in KL. Due to the broad momentum

Table 3. Paired beam settings for three time-of-flight intervals (also called Points).

	TOF interval, ns	muons from runs with P_{D2} (MeV/c)	pions from runs with P_{D2} (MeV/c)
Point 1	27.4 – 27.9	294	362
Point 2	28.0 – 28.6	258	320
Point 3	28.9 – 29.6	222	280

acceptance of the MICE beam line in $\pi \to \mu$ mode, the pions contaminating the muon sample have higher momenta than the muons, in order for the time-of-flight to be consistent [2] (see Figure 4, right).

The pion contamination is studied in positive muon beam runs with nominal beam momentum 200 MeV/c ($p_{D2} = 238$ MeV/c) with a collected statistics of about 270 $\times 10^3$ triggers. The study is performed as a function of the time-of-flight of the beam particles in three distinct time-of-flight intervals (referred to below as "Points 1-3") whose choice is dictated by the availability of calibrations data for which the specified interval is populated mainly by muons or mainly by pions. Pairs of calibration runs for which muons and pions present time-of-flight values within the same range (see table 3) are defined for each point and are used to benchmark the KL response to muons or to pions of given time-of-flight.

Figure 3-a shows the time-of-flight distribution of particles in the MICE muon beam. The examined three Points are highlighted in grey. The widths of the intervals have been determined by taking into account the overlap regions between the calibration runs. In each of these time-of-flight intervals the spectra of the KL response can be extracted for muons and pions separately from the calibration runs. These spectra are then used as templates for the response to muons and pions in that time-of-flight interval for the muon runs. Figure 8 shows examples of the muon and pion templates.

As an example, Figure 6 shows the time-of-flight distributions in two paired beam settings. The interval between 28.0–28.6 ns in the TOF0–TOF1 time-of-flight is populated mainly by muons for one beam setting and by pions for the other. These configurations were also modelled using the Monte Carlo simulations (Figure 7) using the same TOF0–TOF1 time-of-flight interval of 28.0–28.6 ns.

4.2.2 KL detector distributions

In the range 200–300 MeV/c, both muons and pions are minimum ionizing (MIP) particles, but in the KL detector material pions can undergo hadronic interactions as well, which are visible as a tail in the KL response to pions. In order to compensate for light attenuation in the scintillator, the KL response to a particle is defined in terms of the product of the digitised signals from the left and right sides of each slab divided by their sum:

$$ADC_{\text{product}} = 2\,\frac{ADC_{\text{left}} \times ADC_{\text{right}}}{ADC_{\text{left}} + ADC_{\text{right}}},$$

[2] This feature prevents the use of Cherenkov detectors in MICE Step I to fully tag pions, in absence of a precise determination of momentum for beam particles

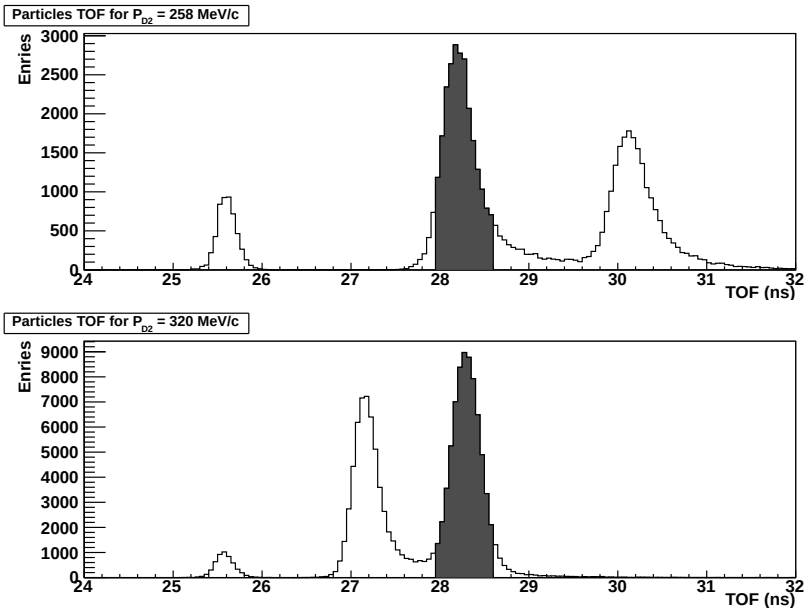

Figure 6. Time-of-flight distributions in two paired beam settings. The interval 28.0–28.6 ns (shaded) is populated by muons (pions) in the upper (lower) plot.

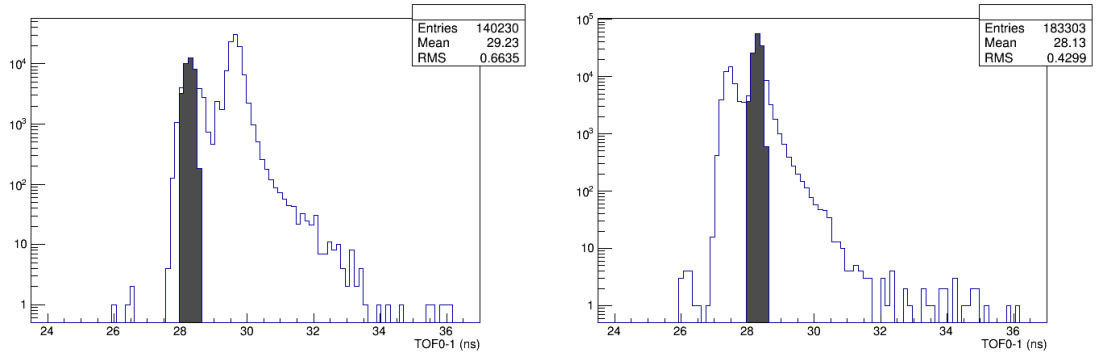

Figure 7. Monte Carlo simulation of the time-of-flight distributions of two paired beam settings. The interval 28.0–28.6 ns (shaded) is populated by muons (pions) in the left (right) plot.

where the factor of 2 is present for normalisation. The products are summed for all slabs in KL above threshold. It can be shown that the used normalized ADC product is the combination of the PMTs signals that is less sensitive to the particle hit position along the fiber length, in presence of two attenuation lengths of which one is much shorter than the other [29], [30].

The KL response to muons and pions in calibration runs and to an unknown particle mix in muon mode are shown in figure 8. The distribution for the pions displays a larger tail than the muon one, reflecting the presence of hadronic interactions. This aspect is used in the following analysis, to estimate on a statistical basis the MICE muon beam contamination.

The digitisation of the KL response was fine-tuned suing the data described in this note. The

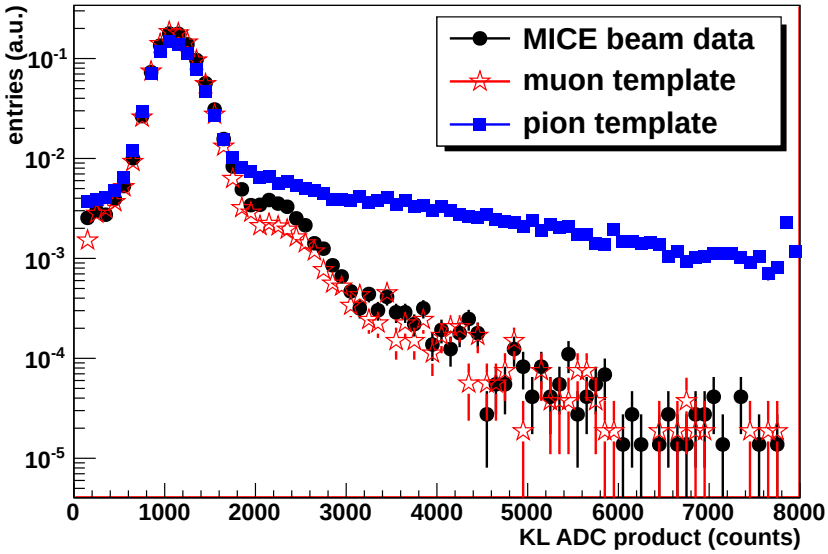

Figure 8. Muon (red stars) and pion (blue squares) templates at Point 2 from calibration runs, compared to MICE muon beam data (black dots). About 30 % of the particles tagged as pions by TOF0–TOF1 decay to muons before KL. Plots are normalised to unity.

correspondence between the ADC peaks in the KL data and the Monte Carlo was carried out by taking into account:

- the smearing of the photons produced in the scintillation fibres, which are assumed to follow Poisson statistics;
- the photoelectrons created at the photocathode, which are also smeared according to Poisson statistics;
- the photomultiplier gain, which is assumed to be Gaussian with the mean equal to the photomultiplier gain ($\sim 2 \times 10^6$) and the standard deviation equal to half of the gain [31];
- the conversion factors from photoelectrons to ADC (250,000 PE/ADC), from MeV to photoelectrons (0.000125 MeV/PE), the two-component scintillating fibre attenuation lengths (2400 mm and 200 mm), the scintillating fibre collection efficiency (3.6%), the light-guide collection efficiency (85%) and the photomultiplier tube quantum efficiency (26%), in order to obtain $\sim$ 1060 ADC counts for a minimum ionising peak.

4.2.3 Analysis with KL and TOF information

This method exploits the information contained in the full KL response spectrum in order to extract the fractions of muons and pions in the MICE beam for each time-of-flight interval. The method employs the ROOT TFractionFitter method [32] based upon [33], treating the muon and pion templates as if they were different Monte Carlo components to be fitted to the actual KL spectrum in

the MICE data. This fit takes into account, through a standard likelihood fit using Poisson statistics, both data and template statistical uncertainties, allowing the templates to vary within statistics.

Due to the different momentum distributions some particles from calibration runs with a given time-of-flight measurement may contribute more (or less) to the final result, than the particles from muon run with the same time-of-flight value. The uneven distributions can be taken into account by reducing the reference time-of-flight intervals, but this approach would require a large statistics. Alternatively weights proportional to the time-of-flight density distributions could be used reweighting the KL response templates by the time-of-flight distribution, to account for the different distributions of this variable for muons or pions in calibration runs and muon runs within the selected interval. Unfortunately the fluctuations of the reweighted templates would not follow the Poisson distribution anymore so this approach cannot be adopted here. Though there are methods to solve this problem [34], in the following this effect is treated as a systematic, whose impact is assessed by splitting into finer intervals the time-of-flight ranges defined in table 3.

Though fitting the full spectrum should in principle provide a better description of the relative muon and pion fractions, it should be noted that, despite the requirement of a single particle in the TOF counters, a two MIPs peak (between 1900 and 2700 counts) is visible in the KL response distribution of figure 8. This is due to pile-up due to the coincidence of two-particle tracks traversing the KL during the integrating period of the electronics and is dependent on the particle rate. The Monte Carlo simulations shown in Figure 9 shows the KL ADC product response for the muon and pion template beams and for a 6π mm· rad, 200 MeV/c pion-muon beam. The second peak from 1900 to 2700 counts can reproduce the data if a XX% pile-up component is added to the Monte Carlo, as is shown in the bottom right plot in Figure **??**.

The fit of the Monte Carlo simulation of the 6π mm· rad, 200 MeV/c pion-muon beam is performed in Figure 10. The fit reproduces the KL ADC product distribution of the pion-muon beam, if the pion contamination in the beam is $(0.3 \pm 0.6)\%$. This is to be compared to the Monte Carlo determination at the KL position of $(0.25 \pm 0.0X)\%$, showing that the method can reproduce the level of contamination expected (both sets of errors are statistical).

Since the second peak depends on the data-taking rate, the template beams and the pion-muon beams had different levels of pile-up. Therefore, the fits to the pion contamination of the pion-muon beams taken with data were performed excluding the ADC product region from 1900 to 2700 counts, The results are shown in figure 11 for Point 2. The pion contaminations obtained with this method are reported in Table 7 for the three points. Errors include both statistical and systematic uncertainties. The sources of systematics and the way their impact is assessed are summarized in table 4.

Table 4. Sources of systematic errors in the evaluation of the pion contamination

Effect	Assessment method	Impact on pion contamination
Time-of-flight distribution	finer subdivision	40%
Time-of-flight calibration	shift calibrations by ± 0.1 ns	3%
Fitted range	vary exclusion region	15%
Histogram binning	double/halve bin sizes	3%

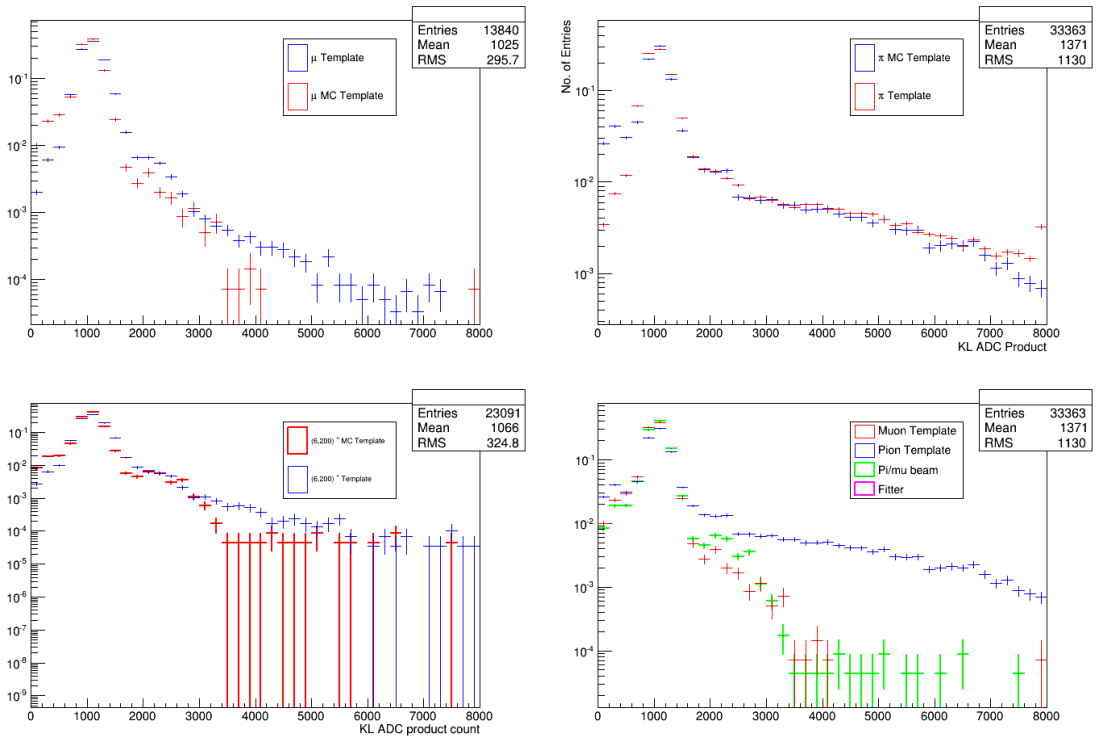

Figure 9. Monte Carlo simulation of the KL ADC product distributions for the muon template (top left), pion template (top right) and for the 6π mm· rad, 200 MeV/c pion-muon beam (bottom left) for data and Monte Carlo. The bottom right plot shows a comparison of the Monte Carlo simulations of the KL ADC product response for the muon, pion and the pion-muon beams. The pion contamination of the latter can be obtained by fitting the pion and muon templates to the distribution.

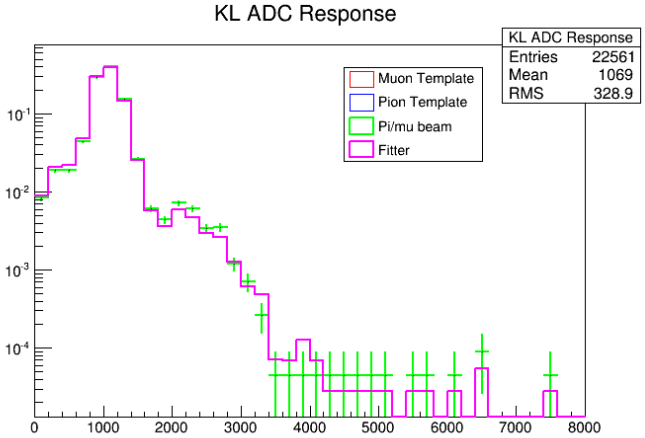

Figure 10. Fit to the KL ADC product distribution of the Monte Carlo 6π mm· rad, 200 MeV/c pion-muon beam. A pion contamination of $(0.3 \pm 0.6)\%$ was obtained from the fit.

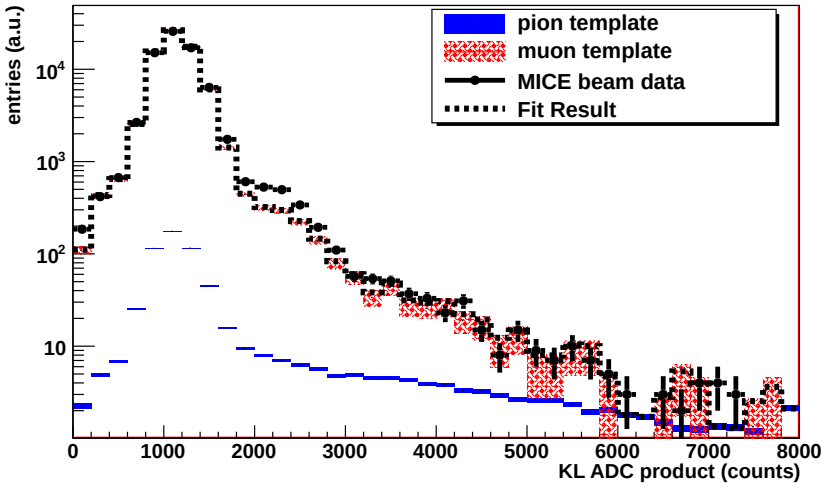

Figure 11. MICE beam data (black dots), muon (red dotted area) and pion (blue solid area) fractions, are normalised to the the template fit (black histogram) performed to the KL product spectrum excluding the window from 1900 to 2700 counts.

4.2.4 Cross-check with a classical method

A simpler method consists in applying a threshold on KL product in order to identify only those pions having hadronic interactions, and counting the fraction of events with KL response above this threshold (see figure 8). This fraction is then expressed as a function of the fractions of muons and pions in paired calibration runs at the same threshold. If in a muon run R^{tot} is the total number of particles and R^{cut} is the number of particles that pass the cut on the KL product, then

$$\begin{cases} R^{tot} = R_\mu + R_\pi \\ R^{cut} = k_\mu R_\mu + k_\pi R_\pi \end{cases}$$

where R_μ and R_π are numbers of muons and pions in the muon run and k_μ and k_π are the fractions of muons and pions in the corresponding calibration runs. R_μ and R_π are then used to extract fraction of muons in the beam, q_μ, and the pion contamination fraction, q_π:

$$q_\mu = \frac{R_\mu}{R^{tot}} \qquad \text{and} \qquad q_\pi = \frac{R_\pi}{R^{tot}}\,.$$

Results are plotted in figure 12 for the three time-of-flight points and for three values of the threshold on the KL product. Table 5 gives all details for Point 2.

An estimate of the systematic pion-contamination uncertainty related to the dependence upon the threshold value is reported in table 6. A second source of systematic uncertainty (muon contamination) results from tails of the muon distribution overlapping the pion time-of-flight peak (see Fig.3). Assuming a contamination of 30% results in a reduction of less than 0.2% of the pion fraction in the muon beam. A third source of systematic uncertainty (difference in TOF distributions) results, as already discussed above, from the differences time-of-flight spectra between

Table 5. Pion and muon fractions in calibration and muon runs for time-of-flight Point 2 for three cuts on KL product: N_μ^{tot} and N_μ^{cut} are numbers of muons, and N_π^{tot} and N_π^{cut} of pions, before and after cut. Uncertainties are statistical only.

KL cut	3000	4500	7000
N_μ^{tot}	53334	53334	53334
N_μ^{cut}	234	53	7
N_π^{tot}	68933	68933	68933
N_π^{cut}	7785	4330	1390
$k_\mu, \%$	0.439 ± 0.029	0.099 ± 0.014	0.013 ± 0.005
$k_\pi, \%$	11.29 ± 0.12	6.28 ± 0.09	2.01 ± 0.05
R^{tot}	72709	72709	72709
R^{cut}	391	92	16
R_μ	72045.8	72389.6	72386.7
R_π	663.2	319.4	322.3
$q_\mu, \%$	99.08 ± 0.52	99.56 ± 0.48	99.56 ± 0.52
$q_\pi, \%$	0.91 ± 0.36	0.44 ± 0.31	0.44 ± 0.36

the analyzed particles and the calibration ones. In this analysis the KL product distributions can be reweighted using the time-of-flight ones, thus making all time-of-flight distributions flat. This approach produces results deviating by less than 0.2% from the default one, without any preferred direction.

The pion contaminations obtained with a KL product cut at 4500 counts are reported in Table 7. Errors include both statistical and systematics uncertainties.

Table 6. Sources of systematic errors in the evaluation of the pion contamination for the cross-check. Values in parenthesis refer to Point 3.

Effect	Assessment method	syst. error
KL threshold value	change of threshold value for KL cut	0.5(1.0) %
μ contamination	μ background in calibration runs	0.2 %
difference in TOF distribution between calibration and μ runs	change reference TOF intervals	0.2 %

4.2.5 Estimation of the pion contamination in the MICE muon beam

Results to estimate the MICE muon beam pion contamination are summarized in table 7. Taking into account the number of beam particles in each TOF interval analyzed (Point 1–3), the pion contamination averages to

$$(1.11 \pm 0.29 \pm 0.32)\%$$

, where the systematic uncertainty includes the small variation, $\pm 0.1\%$, associated to the lack of knowledge of the pion contamination in the time-of-flight intervals in which the analysis was not performed (white area in figure 3-a).

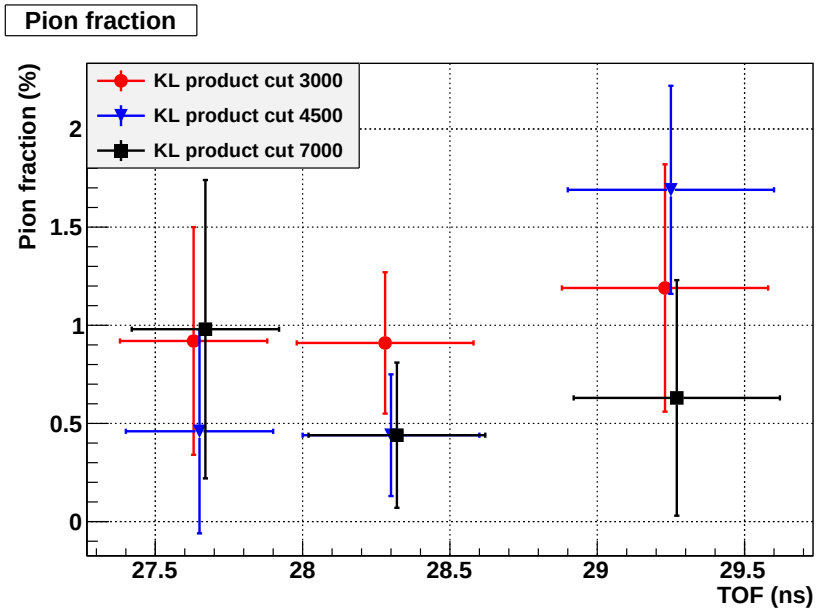

Figure 12. Pion contamination in a muon run for time-of-flight Points 1–3, estimated for three different cuts on KL product (with slight horizontal shifts for clarity). Horizontal bars indicate widths of time-of-flight intervals; vertical error bars are statistical only.

Table 7. Summary of results on pion contamination. The average of the results for Point 1 to 3 takes into account the fraction of particles in each interval. Statistical and systematic errors are reported.

Method	$\pi(\%)$ at Point 1	$\pi(\%)$ at Point 2	$\pi(\%)$ at Point 3 (%)	average π cont. (%)
analysis	$0.65 \pm 0.46 \pm 0.30$	$0.84 \pm 0.27 \pm 0.34$	$1.90 \pm 0.37 \pm 0.80$	$1.11 \pm 0.29 \pm 0.30$
cross-check	$0.46 \pm 0.52 \pm 0.57$	$0.44 \pm 0.31 \pm 0.57$	$1.69 \pm 0.53 \pm 1.04$	$0.81 \pm 0.24 \pm 0.44$
MC				0.33

This number is in agreement with MonteCarlo estimates, taking into account errors (see figure 5) and is compatible to what computed with a simple classical method, used as a cross-check. It translates to a pion contamination of $(0.82 \pm 0.22 \pm 0.24)\%$ at the entrance of the MICE cooling channel (first Focus coil ~ 3.36 m downstream TOF1).

5. Conclusions

The pion contamination in the MICE muon beam has been measured, using precision time-of-flight counters in combination with the KL sampling calorimeter. All measurements are in agreement with contamination at or below the 1% level at the entrance of the cooling channel (~ 3.36 m downstream TOF1). Thus the MICE beam line meets the requirement set for it on pion contamination, in order to demonstrate and characterise ionisation cooling.

Acknowledgements

We gratefully acknowledge the help and support of the ISIS staff and of the numerous technical collaborators who have contributed to the design, construction, commissioning and operation of the experiment. In particular we would like to thank S. Banfi, F. Chignoli, R. Gheiger, A. Gizzi, V. Penna, R. Mazza and W. Spensley. We wish to acknowledge the essential contributions in the conceptual development of a muon cooling experiment made by P. Drumm, R. Edgecock, P. Fabbricatore, R. Fernow, D. Findlay, W. Murray, J. Norem, P.R. Norton, K. Peach, C. Prior and N. McCubbin. We would also wish to acknowledge the work done in the early stages of the experiment by G. Barr, P. Chimenti, S. Farinon, G. Giannini, E. Radicioni, G. Santin, C. Vaccarezza, S. Terzo and K. Tilley. The experiment was made possible by grants from National Science Foundation and Department of Energy (USA), the Istituto Nazionale di Fisica Nucleare (Italy), the Science and Technology Facilities Council (UK), the European Community under the European Commission Framework Programe 7, the Japan Society for the Promotion of Science (Japan) and the Swiss National Science Foundation (Switzerland), in the framework of the SCOPES programme. We gratefully acknowledge their support.

References

[1] A. Blondel *et. al.*, *Proposal to the Rutherford Appleton Laboratory: an international muon ionization cooling experiment (MICE)*, *MICE-NOTE-21* (2003). http://hep04.phys.iit.edu/cooldemo/micenotes/public/pdf/MICE0021/MICE0021.pdf.

[2] D. G. Koshkarev, *Proposal for a decay ring to produce intense secondary particle beams at the SPS*, Tech. Rep. CERN/ISR-DI/74-62, CERN Internal Report, 1974.

[3] S. Geer, *Neutrino beams from muon storage rings: Characteristics and physics potential*, *Phys.Rev.* **D57** (1998) 6989–6997, [hep-ph/9712290].

[4] **Muon Collider/Neutrino Factory** Collaboration, M. M. Alsharo'a *et. al.*, *Recent progress in neutrino factory and muon collider research within the Muon collaboration*, *Phys. Rev. ST Accel. Beams* **6** (2003) 081001, [hep-ex/0207031].

[5] A. Blondel (Ed.) *et. al.*, *ECFA/CERN studies of a European neutrino factory complex*, *CERN-2004-002* (2004).

[6] S. Choubey *et. al.*, *International Design Study for the Neutrino Factory, Interim Design Report*, *IDS-NF-20* (2011) [hep-ex/1112.2853].

[7] F. Tikhonin, *On the effects at colliding mu meson beams*, *JINR-P2-4120* (2008) [hep-ph/0805.3961].

[8] S. Geer, *Muon colliders and neutrino factories*, *presented at 25th International Linear Accelerator Conference (LINAC10), Tsukuba, Japan, 12-17 Sep 2010* (2010).

[9] C. M. Ankenbrandt *et. al.*, *Status of muon collider research and development and future plans*, *Phys.Rev.ST Accel.Beams* **2** (1999) 081001, [physics/9901022].

[10] D. Neuffer, *Principles and applications of muon cooling*, *Part. Accel.* **14** (1983) 75.

[11] S. Ozaki *et. al.*, *Feasibility study 2 of a muon based neutrino source*, *BNL-52623, http://www.cap.bnl.gov/mumu/studyii/FS2-report.html* (2001).

[12] **MICE** Collaboration, D. Adams *et. al.*, *Characterization of the muon beams for the Muon Ionization Cooling experiment*, *submitted to Eur. J. Phys. C* (2013).

[13] R. Bertoni *et. al.*, *The design and commissioning of the MICE upstream time-of-flight system*, *Nucl.Instrum.Meth.* **A615** (2010) 14–26, [hep-ph/001.4426].

[14] M. Bonesini *et. al.*, *Behaviour in magnetic fields of conventional and fine-mesh photomultipliers*, *Nucl.Instrum.Meth.* **A693** (2012) 130–137.

[15] L. Cremaldi, D. A. Sanders, P. Sonnek, D. J. Summers, and J. J. Reidy, *A Cherenkov Radiation Detector with High Density Aerogels*, *IEEE Trans.Nucl.Sci.* **56** (2009) 1475–1478, [hep-ph/0905.3411].

[16] D. Sanders, *MICE Particle Identification Systems*, *Particle Accelerator Conference (PAC09), Vancouver* (2009) [hep-ph/0910.1332].

[17] M. Bonesini, *Progress of the MICE experiment at RAL*, *to be published on Nucl. Phys. B. Proc. Suppl.* (2013) [physics.acc-ph/1303.7363].

[18] M. Ellis *et. al.*, *The design, construction and performance of the MICE scintillating fibre trackers*, *Nucl. Instr. Meth* **A659** (2011) 136–159, [physics.ins-det/1005.3491].

[19] **MICE** Collaboration, M. Bogomilov *et. al.*, *The MICE Muon Beam on ISIS and the beam-line instrumentation of the Muon Ionization Cooling Experiment*, *JINST* **7** (2012) P05009, [1203.4089].

[20] R. Bertoni *et. al.*, *The Construction of the MICE TOF2 detector*, *MICE-NOTE-DET-286* (2010).

[21] F. Ambrosino *et. al.*, *Calibration and performances of the KLOE calorimeter*, *Nucl.Instrum.Meth.* **A598** (2009) 239–243.

[22] G. Gregoire *et. al.*, *MICE Technical Report*, tech. rep., Rutherford Appleton Laboratory, 2005. http://www.mice.iit.edu/trd/MICE-Tech-ref.html.

[23] C. Booth *et. al.*, *The design, construction and performance of the MICE target*, *JINST* **8** (2013) P03006, [1211.6343].

[24] S. Blot *et. al.*, *Proton Contamination Studies in the MICE Beam Line*, *Proc. IPAC11* (2011).

[25] R. Bertoni *et. al.*, *Analysis of PID detectors (TOF and KL) performances in the MICE 2010 run*, *MICE-NOTE-DET-337* (2011).

[26] M. Bonesini *et. al.*, *The Refurbishing of MICE TOF0 and TOF1 detectors*, *MICE-NOTE-DET-363* (2012).

[27] T. Roberts, "G4beamline, A Swiss Army Knife for Geant4, optimized for simulating beamlines." http://g4beamline.muonsinc.com.

[28] "MICE Analysis User Software (MAUS) ." http://micewww.pp.rl.ac.uk/projects/maus/wiki.

[29] **KLOE** Collaboration, A. Di Domenico, *Kloe internal note 196*, .

[30] **HARP** Collaboration, U. Dore, *private communication*, .

[31] H. H. Tan, *A statistical model of the photomultiplier gain process with applications to optical pulse detection*, *The Telecommunications and Data Acquisition Progress Report* **42-68** (1982). http://ipnpr.jpl.nasa.gov/progress_report/42-68/68H.PDF.

[32] R. Brun and F. Rademakers, *ROOT - An Object Oriented Data Analysis Framework*, *Nucl. Instrum. Meth.* **389** (1997) 81–86.

[33] R. Barlow and C. Beeston, *Fitting using finite Monte Carlo samples*, *Comp. Phys. Commun.* **77** (1993) 219–22.

[34] L. Caminada, *Study of the Inclusive Beauty Production at CMS and Construction and Commissioning of the CMS Pixel Barrel Detector*, *Springer* (2012).